Ionospheric effects upon a satellite navigation system at Mars

Michael Mendillo,[1] Xiaoqing Pi,[2] Steven Smith,[1] Carlos Martinis,[1] Jody Wilson,[1] and David Hinson[3]

Received 9 July 2003; revised 27 January 2004; accepted 3 March 2004; published 30 April 2004.

[1] Trans-ionospheric radio propagation effects resulting in ranging errors are examined for a potential orbital network of communications and navigational satellites at Mars. Using recent results from the radio science experiment on board the Mars Global Surveyor (MGS) spacecraft and a photochemical model of Mars' ionosphere, we study the total electron content (TEC) at Mars to investigate how its latitude, local time, and solar cycle patterns would contribute to errors in positioning on the planet. In addition, we examine the relationship between TEC and peak density (N_{max}) and find that their ratio, called the equivalent slab thickness, shows that integral preserving distortions of the $N_e(h)$ profile can be rather substantial, implying that neutral atmosphere dynamics can have strong effects upon Mars' photochemical ionosphere. We use MGS observations to validate modeling results and determine the extreme cases for TEC at Mars (i.e., when the planet is at perihelion during solar maximum years and at aphelion during solar minimum years). If a proposed Mars Communication and Navigation (MC&N) System used UHF/L-band (1–2 GHz) transmission frequencies similar to those used for the terrestrial Global Positioning System (GPS) satellites, upper limits to the magnitude and variability of the martian ionosphere (TEC $< \sim$few $\times 10^{16}$ el m^{-2}, with $\sigma \sim 10\%$) would not be of concern unless extremely precise positional information were required (<1 m). The impact of the ionosphere would be greater along slanted ray paths, and especially if lower frequency UHF beacon frequencies (e.g., 400 MHz) were selected for use. Indeed, such effects could be used as a diagnostic for the global structure of Mars' ionosphere, much in the same way as GPS measurements are used in terrestrial ionospheric physics. *INDEX TERMS:* 6225 Planetology: Solar System Objects: Mars; 5435 Planetology: Solid Surface Planets: Ionospheres (2459); 5494 Planetology: Solid Surface Planets: Instruments and techniques; 6934 Radio Science: Ionospheric propagation (2487); *KEYWORDS:* ionosphere, satellite navigation, Mars

Citation: Mendillo, M., X. Pi, S. Smith, C. Martinis, J. Wilson, and D. Hinson (2004), Ionospheric effects upon a satellite navigation system at Mars, *Radio Sci.*, *39*, RS2028, doi:10.1029/2003RS002933.

1. Introduction: Terrestrial Ionosphere and GPS Impacts

[2] A planet's ionosphere imposes a delay upon the radio transmissions from an orbiting artificial satellite to a ground receiving station, thus leading to ranging errors in systems designed for precise positioning. This is a well-studied effect on Earth for the Global Positioning System (GPS) used in an ever-increasing spectrum of civilian and military applications. Illustrated schematically in Figure 1a is the augmented GPS system used for air travel across the continental United States (CONUS). The terrestrial ionosphere typically exhibits rather smooth variations in latitude and local time across CONUS, but dramatic and very structured disturbances can occur during periods of increased solar and geomagnetic activity. Technically, the ionospheric delay effect could be eliminated by operating the system with dual-frequency signals transmitted by the satellites. Otherwise, either real-time measurements of the ionosphere or reliable models of its temporal and spatially dependent behavior are needed to correct for "group path delay effects" that could lead to errors in the determination of aircraft location.

[1]Center for Space Physics, Boston University, Boston, Massachusetts, USA.
[2]Jet Propulsion Laboratory, California Institute of Technology, Pasadena, California, USA.
[3]Department of Electrical Engineering, Stanford University, Stanford, California, USA.

0048-6604/04/2003RS002933$11.00

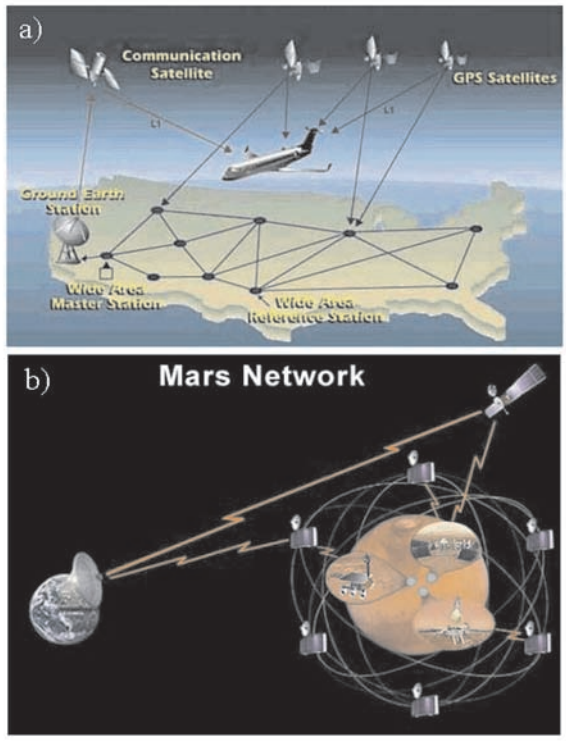

Figure 1. (a) An illustration of the use of the Global Positioning System (GPS) satellites for precise location and navigation of aircraft over the continental United States (CONUS). Depicted schematically is a network of reference stations (currently 25 in number) that form the Wide Area Augmentation System (WAAS) of the Federal Aviation Administration (FAA). Satellite radio transmissions to aircraft and ground sites traverse the terrestrial ionosphere and suffer retardation effects that lead to range errors, if not corrected for the total electron content (TEC) of the ionosphere along each ray path. (Figure courtesy of the FAA.) (b) A schematic illustration of a proposed Mars Network for communications and navigation. Several such concepts are under study, and ionospheric corrections for the TEC on Mars depend on the final selection of frequencies to be used. (Figure courtesy of NASA/JPL.)

[3] For the terrestrial case, the nominal configuration for GPS involves 24 satellites (and up to 6 in-orbit spares) at an altitude of about 20,200 km in 6 orbital planes in order to have at least 4 satellites available at any time from any place to determine a receiver's location. The slanted paths from the receivers to the satellites thus traverse great distances and sample the ionosphere in several directions. The ionospheric parameter of relevance is the integral of electron density along these paths (s), called the slant total electron content,

$$\mathrm{STEC} = \int_r^s N_e(s)ds \qquad (1)$$

While the limits of the integral in equation (1) extend from the receiver to the satellite height, in practice most of the ionosphere is well below GPS heights, and thus an integral to ~2000 km captures most of the electron content. This is fortunate from the perspective of modeling since ionospheric structure to such altitudes involves a set of physical processes and computational methods somewhat different from those needed to model plasma in the inner magnetosphere (or plasmasphere) where the GPS satellites actually reside.

[4] In both scientific investigations and practical applications, it is the vertical TEC that is most frequently used as the standard measure of geographical structures and temporal patterns, rather than the line-of-sight (LOS), i.e., slant TEC, that comes from most satellite beacon observations. This requires a conversion from the LOS measurements to an equivalent vertical TEC. In practice, this is carried out with the assumption that the ionosphere is spatially constant over the region traversed by the ray path. While this is not a bad assumption if the zenith angle (χ) to the satellite is not too large, e.g., $<60^\circ$, such a conversion can introduce errors at low elevation angles when horizontal gradients in the ionosphere are present. Strong spatial gradients do occur in the terrestrial ionosphere, e.g., over longitudes spanning the dawn and dusk local time periods, and in latitude regions where strong electrodynamical processes and/or auroral particle precipitation modify the local, solar produced ionosphere. While very severe gradient effects can be used in computer simulations to show that slant contents fail to capture true quantitative patterns, in practice, slant measurements through and outside regions of large gradients do portray the basic geophysical morphologies being sampled (e.g., see the trough studies in *Mendillo et al.* [1974]). However, to our knowledge, no simple algorithm is currently available to take these gradient effects into account in operational conversions from LOS to vertical TEC, i.e., unless very sophisticated modeling is applied. Thus employing the "horizontal uniformity" assumption for individual satellite-to-receiver ray paths remains the standard, and it allows the local ionosphere to be represented by a single electron density profile with a single vertically integrated total electron content (TEC). For such conditions, the relation between STEC and TEC is simply

$$\mathrm{STEC} = \mathrm{TEC}\sec(\chi) \qquad (2)$$

and the vertical TEC parameter becomes the target to observe or model. The units chosen to describe TEC are

most often in metric column contents of 10^{16} el m^{-2}, called a "TEC unit" or TECU. The lowest TEC values on Earth (~2 TECU) occur during winter nighttimes at subauroral ("*F* region trough") latitudes during solar minimum, and the largest ones (~200 TECU) can be found during solar maximum periods at latitudes within 20° of the geomagnetic equator, in regions called the Equatorial Ionization Anomaly (EIA) or the Appleton Anomaly crests [see *Rishbeth and Garriott*, 1969]. For the GPS satellite L1 frequency (1.57542 GHz), such TEC values correspond to ~0.32 to ~32 m of vertical equivalent range errors, respectively. Such values are of considerable concern to precise positioning and navigational systems, and thus considerable research efforts are underway in real-time monitoring of the ionosphere, numerical modeling of its behavior, and methods of forecasting during both geomagnetically quiet and disturbed periods [e.g., *Pi et al.*, 2003].

2. Case at Mars

2.1. Overview

[5] The operational system illustrated in Figure 1a offers ideas to examine in plans for upcoming explorations of Mars. With a series of orbiters, landers, and rovers planned for the upcoming decades, including sample gathering and return missions, there is an obvious need for positioning and navigation of, as well as communications between, spacecraft and vehicles on the surface of Mars. Requirements are far more rigorous than used in NASA's initial attempts to explore the planet's surface with the Viking Landers in 1976. Moreover, several international programs (both joint and independent from U.S. plans) are underway, and thus the overall problem of positioning and communications could become rather complex. In Figure 1b we show an illustration of concepts being discussed for Mars, ideas not too dissimilar from those proposed in the 1970s that resulted in the now operational GPS systems on Earth. All of the proposed solutions involve some sort of multisatellite network, with the eventual design accepted for the Mars Communications and Navigation (MC&N) system still very much under study [e.g., *Cesarone et al.*, 1999; *Ely et al.*, 1999; *Hastrup et al.*, 1999].

[6] In addition to trans-ionospheric navigational and communications issues, there are other impacts of Mars' ionosphere upon radio propagation scenarios that have been treated in recent studies. *Melnik and Parrot* [1999] discussed propagation scenarios of possible ELF-VLF waves in the martian ionosphere. *Witasse et al.* [2001] have examined how meteoritic layers in the martian ionosphere would affect the attenuation of HF signals. *Safaeinili et al.* [2003] examined how the ionosphere would impact an orbital radar designed to sound subsurface stratigraphy using low frequencies (HF), a system that would also serve as an ionospheric topside sounder. *Armand et al.* [2003] examined distortion effects caused by the ionosphere upon the radar pulses from such a system. The present study is thus one in a growing number linked to understanding the overall influence of Mars' ionosphere upon radio systems.

2.2. Observations of the Ionosphere at Mars

[7] In comparison to Earth, observations of ionospheric profiles at Mars are extremely rare. A comprehensive literature search (summarized in Table 1 of *Mendillo et al.* [2003]) shows that a total of 433 $N_e(h)$ profiles are available for Mars. These were obtained over a 13-year period involving 10 missions from the United States and USSR. Spanning wide ranges of local time, latitude and solar flux conditions, these 433 profiles do not represent the type of comprehensive database that could be used to construct an empirical, global model of the martian ionosphere. Only two of those profiles were made by actual vertical measurements (via the in situ probes on board the Viking landers); the rest were made by radio occultation experiments between satellites at Mars and ground receiving stations at Earth. The earliest of those measurements pioneered the use of radio occultation observations for planetary ionospheres [see *Fjeldbo et al.*, 1966; *Kliore*, 1992; *Schunk and Nagy*, 2000].

[8] The most recent use of the radio occultation method at Mars involves the ongoing observations being made by the radio science (RS) experiment on the Mars Global Surveyor (MGS) satellite [*Hinson et al.*, 1999, 2001]. Briefly, the MGS/RS experiment uses an onboard X-band transmitter (at 8.423 GHz) that is received on Earth as the satellite emerges from or proceeds into its orbit segments behind Mars. The signal is refracted initially by high altitude ionospheric plasma and then by the neutral atmosphere at lower heights. These "angle of arrival" observations are then inverted to yield electron density profiles and neutral temperature profiles, respectively.

[9] For the MGS ionospheric retrievals, there are no a priori assumptions about the shape of the electron density profile, or its peak density; the electron density is assumed to be zero below 90 km. Consistent with practices for terrestrial TEC data, the assumption is made of no horizontal $N_e(h)$ gradients along the path traversed by the signal. The standard deviation of the measurements varies among the experiments, with a typical value of several 10^3 el cm^{-3}. Finally, we note that the geometrical properties of such limb-probing observations impose limitations on the local time coverage possible from occultation measurements (e.g., when Mars is at opposition, most of the samplings occur near dawn and dusk). These are times when solar illumination effects are

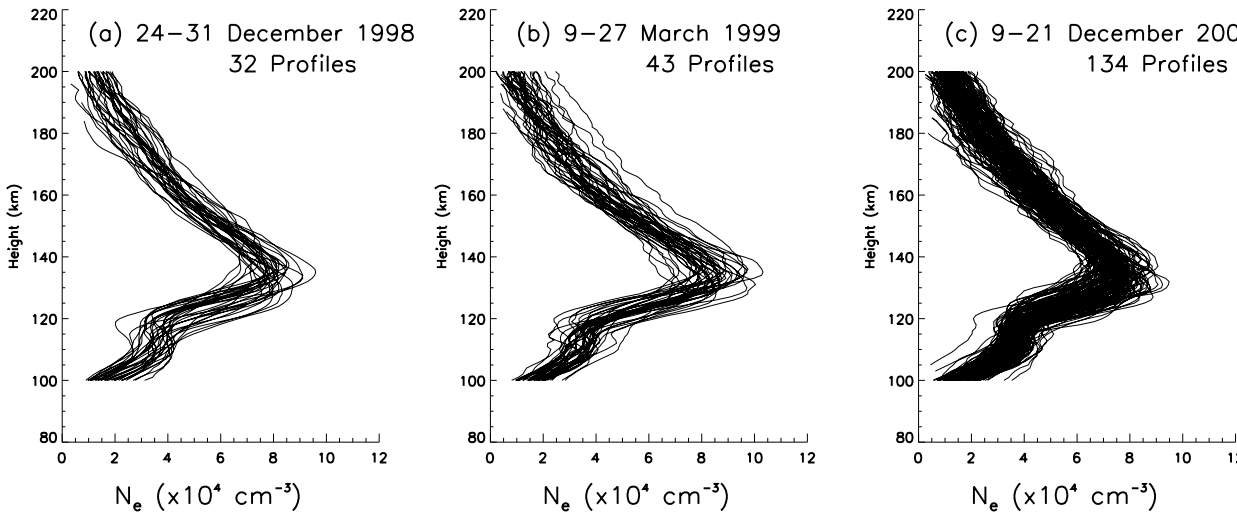

Figure 2. Electron density versus altitude profiles from the radio science experiment on board the Mars Global Surveyor satellite. See Table 1 for observational specifics. For each of these three periods, the total electron content (TEC) parameter is formed by the vertical integration of the profiles shown.

changing rapidly at low latitudes, or minimally at polar latitudes, and thus not ideal cases for data-model comparisons. Yet, the remote diagnostic of a planetary ionosphere remains a remarkable observational achievement and, as we shall discuss below, modeling studies can be used to relate measurements at one point to their global context.

[10] To illustrate the types of ionospheric structure that would be of concern to any MC&N system, shown in Figure 2 are several examples of $N_e(h)$ profiles obtained from the MGS radio science experiment. The observational parameters for these three initial periods of MGS ionospheric measurements are given in Table 1. Note, in particular, that the MGS orbit resulted in occultation data only in the early morning hours and at high latitudes. There are several features to note about the $N_e(h)$ profiles in Figure 2. Firstly, most of the ionosphere falls within the ~100 to ~200 km altitude range, a span about a factor of ten smaller than the physical extent of the terrestrial ionosphere and, on a percentage basis, ~10% versus 30% of their respective planetary radii. The peak electron density occurs near 135 km, with a secondary peak near 110 km. At these altitudes, the density of the neutral atmosphere at Mars is comparable to that found in the terrestrial *E* region, and thus photochemical processes (i.e., solar production, chemical loss and no plasma transport) are sufficient to describe the first-order behavior of Mars' ionosphere (as described recently by *Mendillo et al.* [2003, and references therein]).

[11] There is quite a bit of variability in the profiles in Figure 2, both in the electron density values and in the heights of their maxima. Some of the variability in height arises from longitude effects in the neutral atmosphere at the same local time, as the MGS occultation paths sample several locations on Mars during a day [*Bougher et al.*, 2001]. Yet, simple changes in height of a neutral atmosphere do not result in changes in peak electron density since (for a photochemical layer) the peak density occurs near unit optical depth, wherever that might be in altitude. Changes in solar flux, however, do have a direct effect.

Table 1. MGS/Radio Science Ionospheric Profiles for the Three Periods of Study

Date	Number of Profiles	Latitude Coverage	Longitude Coverage	Local Time, h	Solar Zenith Angle	Ls[a]
24–31 Dec. 1998	32	64.7°–67.3°	all	4.3–3.3	78.4°–80.8°	74.1°–77.3°
9, 11–27 March 1999	43	73.3°–69.7°	26.5°–273.0°	3.6–4.1	76.5°–77.8°	107.6°–115.9°
9–21 Dec. 2000	134	67.5°–69.6°	all	2.8–2.8	80.5°–82.2°	86.8°–92.5°

[a]The solar longitude (Ls) is the angular measure of the orbital position of Mars about the Sun (Ls = 0° or 180° at equinox; Ls = 90° at northern summer solstice; Ls = 270° at southern summer solstice).

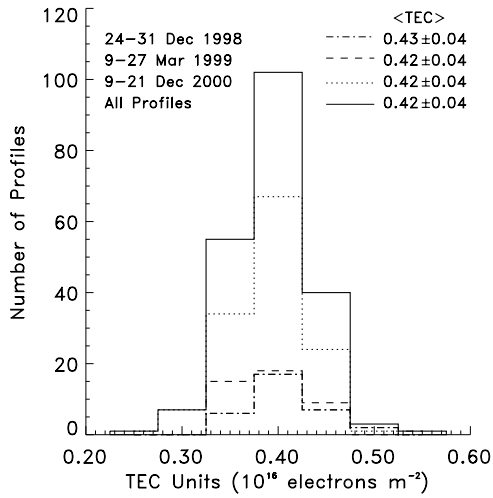

Figure 3. The distribution of martian TEC values from the three $N_e(h)$ data sets shown in Figure 2.

Hantsch and Bauer [1990] discussed solar cycle changes observed in Mars' ionosphere (a topic treated here via modeling in a later section). *Mendillo et al.* [2003] addressed the day-to-day variability in electron density observed at both Mars and Earth in March 1999 (Figure 2b), a period when Mars was near opposition and thus solar flux variability would affect ionospheric variability simultaneously at both planets. For their photochemical layers (e.g., *E* layer for Earth and main peak for Mars), classic Chapman Theory [*Rishbeth and Garriott*, 1969] shows that the equilibrium case has the square of electron density proportional to solar flux. The patterns observed in *Mendillo et al.* [2003] are as follows:

$$[N_m(\text{Mars})]^2 = 0.033 \times \text{E10.7} + 2.8\left(10^9\ \text{e}^-/\text{cm}^6\right) \tag{3a}$$

$$[N_E(\text{Earth})]^2 = 0.100 \times \text{E10.7} + 14.2\left(10^9\ \text{e}^-/\text{cm}^6\right) \tag{3b}$$

where E10.7 is in solar flux units (similar in magnitude to F10.7 flux units), but an index tuned to the solar EUV and X-ray emissions actually responsible for ionization processes [*Tobiska et al.*, 2000; *Tobiska*, 2004]. Detailed numerical modeling of day-to-day variability in the martian ionosphere using the full solar irradiance values appropriate for this period is given in *Martinis et al.* [2003].

2.3. Total Electron Content of the Martian Ionosphere

[12] To determine TEC values from the $N_e(h)$ profiles in a consistent way, we performed the integration in equation (2) from 100 km to 200 km. There are very low electron density values below, and especially above, these heights that cannot be retrieved accurately via the inversion of MGS radio occultation measurements, and these would contribute to the actual TEC value at a given time. The topside ionosphere at Mars often exhibits a sharp termination called "the ionopause" [*Kliore*, 1992; *Vignes et al.*, 2000] in the 300–500 km region, and thus an additional topside segment with $N_e < \sim 10^4$ el cm^{-3} would contribute to the true TEC integral. Holding these topside and bottomside corrections aside for the moment, the major contributions to TEC are shown for the three data periods in Figure 3. There is a remarkable consistency in the TEC values and their ranges. The value of ~0.42 TECU is thus representative of this ~03–04 LT period and latitude range on Mars. Adding small corrections for the contributions below 100 km (~0.02 TECU) and above ~200 km (~0.2 TECU), gives us an overall estimate of, perhaps, 0.7 TECU for the conditions sampled.

[13] To the terrestrial ionospheric physicist, such a small value is within the error of terrestrial TEC values, and certainly of little consequence for GPS applications. What are the implications for the situation on Mars? To address this issue quantitatively, we show in Figure 4 the relationship between range error (ΔR) and TEC magnitude derived from the radio time retardation dependence with frequency relationship [*Hargreaves*, 1992],

$$\Delta R = 0.403 \frac{\text{TEC}}{f^2} \tag{4}$$

where TEC is measured in TECU (10^{16} el m^{-2}), f is in GHz, and ΔR is in meters.

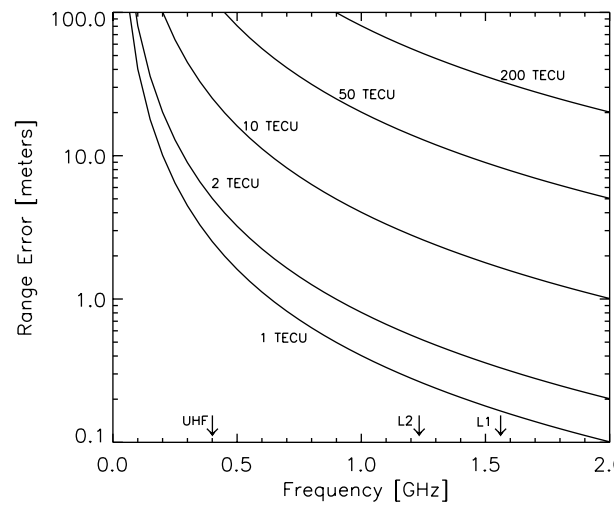

Figure 4. Calculations of ionospherically imposed range errors for vertical TEC versus the frequency used in a satellite navigation system. The arrows indicate a typical UHF (400 MHz) choice, as well as the L1 and L2 frequencies of the terrestrial GPS system.

[14] If a Mars Communications and Navigation system were to adopt GPS frequencies, the martian ionosphere with ~1 TECU would cause about 0.16 m of range error (for GPS L1 radio link), probably of little consequence to mission managers. For an UHF signal of 400 MHz, however, the martian case of ~1 TECU corresponds to a range error of about 2.5 m. This number would be increased by the sec(χ) factor in equation (2) that would be involved in slant ray path scenarios, e.g., in the low elevation-angle views needed for the positioning of surface rovers.

[15] As part of the planning process for a MC&N system, for which estimates of ionospheric range delays are an important element, one must ask how restrictive a view of Mars' ionosphere comes from the profiles in Figure 2 and their TEC values in Figure 3. To do this, we turn to modeling estimates.

3. Simulations of the Mars Ionosphere for Total Electron Content Estimates

[16] While no prior modeling efforts have dealt specifically with the TEC at Mars, there is a rich literature describing the fundamental photochemical processes that create the vertical profiles of ion composition (and therefore electron density) at Mars. Recent summaries of modeling work appear in *Schunk and Nagy* [2000], *Krasnopolsky* [2002], and *Martinis et al.* [2003]. Briefly, Mars has the unusual case of a planet's ionosphere having as its major ion a species not represented in its neutral atmosphere. Thus, while carbon dioxide (CO_2) is by far the dominant neutral gas to be ionized, subsequent and rapid ion-neutral chemistry with trace amounts of atomic oxygen (O) transform the plasma to a molecular oxygen ion (O_2^+) dominated ionosphere. As shown in *Nagy and Cravens* [2002], the main chemical reactions that determine the major ion species are as follows:

$$CO_2 + h\nu \rightarrow CO_2^+ + e^- \quad (5a)$$

$$CO_2^+ + O \rightarrow O_2^+ + CO \quad (5b)$$

$$\rightarrow O^+ + CO_2 \quad (5c)$$

$$O^+ + CO_2 \rightarrow O_2^+ + CO \quad (5d)$$

The dominate loss process for ion-electron pairs is

$$O_2^+ + e^- \rightarrow O + O \quad (5e)$$

With plasma diffusion not an important process below 200 km, the MGS profiles shown in Figure 2 are well described by photochemistry alone, as above, and the electron density structure with height is essentially equivalent to profiles of O_2^+ versus height.

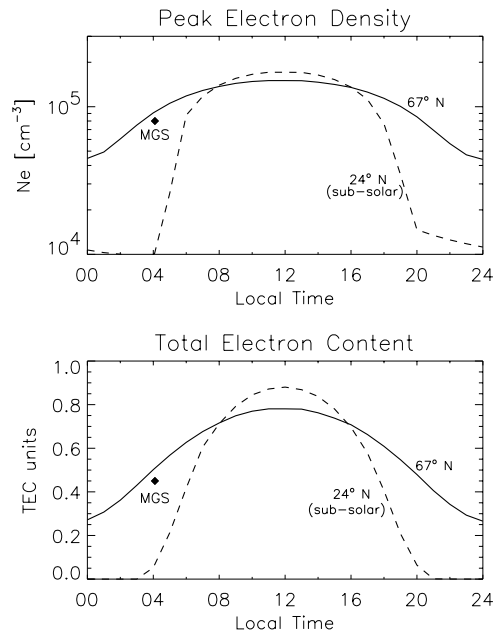

Figure 5. Photochemical model results for the peak electron density (top) and total electron content (bottom) used to place MGS observations in December 1998 into the context of diurnal and latitude behavior on the planet. The solid lines give simulation results at the latitude of MGS data, and dashed lines give results for the subsolar latitude. In both panels, the diamonds represent the average value for N_{max} and TEC obtained from the left panel in Figure 2 (see text).

[17] We now turn to the fact that all of the $N_e(h)$ profiles shown in Figure 2 were obtained under solstice conditions on Mars, at latitudes with sunlight present at large zenith angles for the full day. For such a case, the diurnal variation of a photochemical layer is not too dramatic. This can be shown using the model described in *Martinis et al.* [2003], one that used a more comprehensive set of photochemical equations (20 in number) than summarized above in equations (5a)–(5e), and neutral atmosphere profiles taken from *Fox et al.* [1995]. The results are given in Figure 5. In the top panel, the peak electron density is shown for the average solar conditions for 24–31 December 1998, the initial period of MGS radio science occultation observations. Simulation results for two locations are given: latitude 67°N where the MGS data were taken near 04 LT (shown by the solid line), and at 24°N, the latitude of the subsolar point on Mars, where the maximum electron densities on the planet would occur (shown by the dashed line). The first feature to notice is

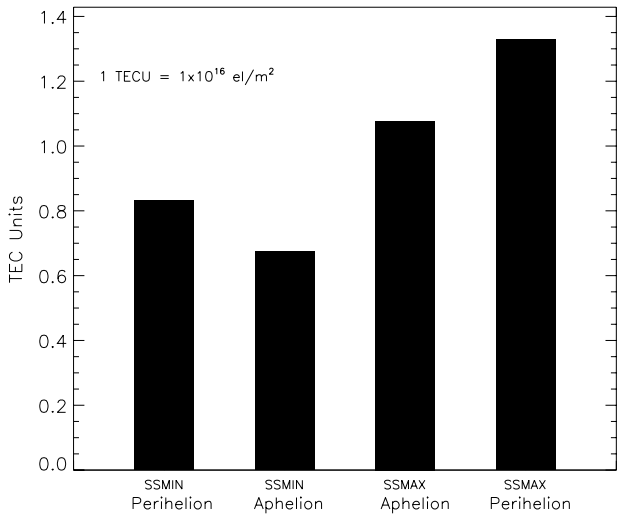

Figure 6. Model results for noontime ionospheric TEC in the altitude range 100–200 km at the subsolar latitude on Mars, for aphelion/perihelion positions during solar min/max conditions.

the very mild gradient in latitude for peak electron density. The noontime value of N_{max} for a solar zenith angle of 0° is only slightly higher than the noontime value for a SZA of 42° at the high latitude site. This reflects the small dependence upon zenith angle in the Chapman equations for a photochemical (α-Chapman) layer.

$$N_{max} = [(P/\alpha)\cos\chi]^{0.5} \quad (6)$$

where P is the peak production rate for an overhead Sun and α is the recombination coefficient (for an in-depth discussion of this point, see the recent terrestrial *E* layer model of *Titheridge* [2000]). For the two simulation values of N_{max} shown in Figure 5, a cosine fit results in an exponent equal to 0.55, essentially consistent with the simple theory embodied in equation (6).

[18] At the subsolar site (representative of all low-to-mid latitudes for diurnal behavior), the familiar rise and decay of a photochemical layer at sunrise and sunset are seen in the dashed-line curve. The diurnal variation is over a factor of 40 at this location. At the "arctic circle" location sampled by MGS, however, the Sun does not set and thus the photochemical layer persists at all local times. The diurnal variation there is only a factor of 4. The value of N_{max} at ~04 LT obtained from MGS is shown by diamonds and falls somewhat below the simulation results (solid line). This is due to several simplifying assumptions used in the model, the primary one being a constant neutral atmosphere in space and time over the planet. Yet, the results do address satisfactorily the specific question we posed, namely, the relationship between the MGS observations at high latitudes and early local times to the maximum levels of ionospheric densities elsewhere on the planet. With model validation obtained at the MGS observation point (where the geometry for photochemistry is the most demanding to handle), we have a high level confidence in model results elsewhere on the planet.

[19] The bottom panel in Figure 5 gives the simulation results for the total electron content (TEC) at the MGS and subsolar latitudes. As would be expected, the diurnal behavior for TEC is similar to that for peak density, and the diurnal range is again nearly a factor of 4. The model's small TEC shortfall at the comparison point with the MGS observations occurs from the same limitations described above for peak density. In addition, there is considerable uncertainty for the photo-electron secondary ionization rate that contributes to bottomside peak densities that contribute to TEC (see *Martinis et al.* [2003] for full model details). Still, the agreement is rather good and we proceed in using the model to estimate the ranges possible for the maximum TEC on Mars throughout a typical solar cycle. To do this, we stay at the subsolar point and run the model for the extreme cases of Mars at perihelion and aphelion at times of solar minimum and maximum. The solar min/max neutral atmospheres come from *Fox et al.* [1995] and the solar irradiance patterns from the SOLAR 2000 model of *Tobiska et al.* [2000]. The results of these four case studies are shown in Figure 6. The full solar cycle range for daytime TEC in the 100–200 km altitude range is thus ~0.7 to ~1.4 TECU. As pointed out earlier, on Earth the variation of TEC over a solar cycle would be one to two orders of magnitude larger, not so much due to the Earth's closer distance to the Sun, but to the nature of a nonphotochemical layer (*F2*) providing the major contribution to the TEC integral. The overall results from photochemical model studies thus point to the TEC on Mars exhibiting only minor latitude gradients, longitude gradients determined only by solar terminator effects at dawn and dusk, and minimal solar cycle variations. Variations from this somewhat bland ionospheric morphology might occur during times of variability in the neutral atmosphere, e.g., due to local topography and/or dust storms [*Forbes*, 2002], or during episodic bursts in solar wind impact upon the planet. Finally, in the southern hemisphere, where localized crustal magnetic fields occur in far greater proportion than in the northern hemisphere, local modifications to simple photochemical ionospheric behavior might be significant, as will the differential hemispheric impact of

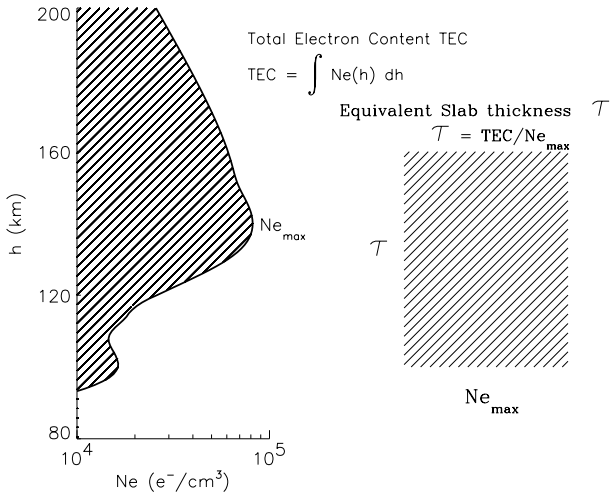

Figure 7. Illustration of three parameters used to characterize an ionospheric $N_e(h)$ profile: N_{max}, TEC, and equivalent slab thickness τ.

solar wind effects upon the ionopause [*Vignes et al.*, 2000; *Ma et al.*, 2002].

4. Changes in the Equivalent Slab Thickness of the Martian Ionosphere

[20] It is often useful to create a first-order representation of an ionosphere by a single slab of plasma. For the terrestrial case of ionospheric corrections to GPS signals, this is, in fact, the current method adopted by a host of operational users. Such a representation of an ionosphere by its so-called equivalent slab thickness (τ) is illustrated in Figure 7. If the TEC were to result from a layer with electron density uniformly equal to the peak density, the resulting slab thickness can be a useful way to describe the first order shape (i.e., breadth) of the $N_e(h)$ profile. In the terrestrial case, τ varies in space and time far less dramatically than either of its parameters (N_{max} and TEC), and thus empirical models for τ can be used in various world regions for specification of TEC when ionosonde measurements of N_{max} are the only observable available [*Fox et al.*, 1991]. As a scientific parameter, τ can be used to study the behavior of atmospheric scale heights, and thus neutral temperature effects [*Titheridge*, 1973].

[21] Could a slab thickness representation be a useful tool in specifications of the ionosphere on Mars? Since the ionospheric database for Mars is far from complete, regionally or globally, it is instructive to examine how slab thickness on Mars represents the local ionosphere at the MGS measurement points. For the three data sets shown in Figure 2, the resulting slab thickness values are shown in histogram form in Figure 8. A comparison of the TEC statistics in Figure 3 with the slab thickness results in Figure 8 reveals that the τ variabilities are slightly larger than the TEC variabilities ($\sim$11% versus 9%), suggesting that changes in shape of the ionosphere on Mars are linked to changes in N_{max}. Thus, in Figure 9, we explore the correlation of slab thickness versus peak density. There is a clear trend of the ionosphere becoming thinner as the peak density increases. The trend is rather pronounced in the December 1998 set of MGS profiles, but also clearly apparent in the March 1999 and December 2000 data as well.

[22] The message we obtain from Figure 9 is that the ionosphere on Mars exhibits an equivalent slab thickness pattern that is different from that seen on Earth where, to first order, N_{max} and TEC are highly correlated [*Fox et al.*, 1991], with variabilities of $\sim$25% [see also *Rishbeth and Mendillo*, 2001]. For Mars, τ appears to be related to its peak density in a far more coupled manner: to first order, the TEC is constant with shape-distorting (but integral-preserving) variabilities in the $N_e(h)$ profiles. The cause of such effects in a layer where plasma diffusion is not important remains unclear. A photochemical regime can change only if the solar irradiance changes or the neutral atmosphere upon which it operates changes. In Figure 10, we show the effects of solar input for the extreme cases of Mars at aphelion during solar minimum versus perihelion during solar maximum (i.e., the $N_e(h)$ profiles used to generate the extreme TEC cases (second and fourth histogram values) shown in Figure 6). For photochemical-only processes, it is clear that a $N_e(h)$ profile broadens with increasing N_{max}

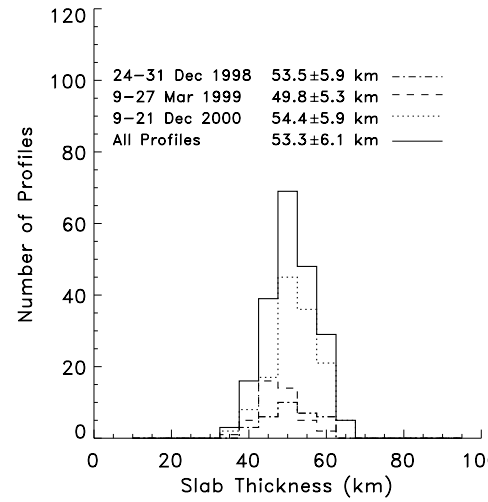

Figure 8. Distribution of the equivalent slab thickness values for Mars' ionosphere derived from the three sets of MGS data shown in Figure 2.

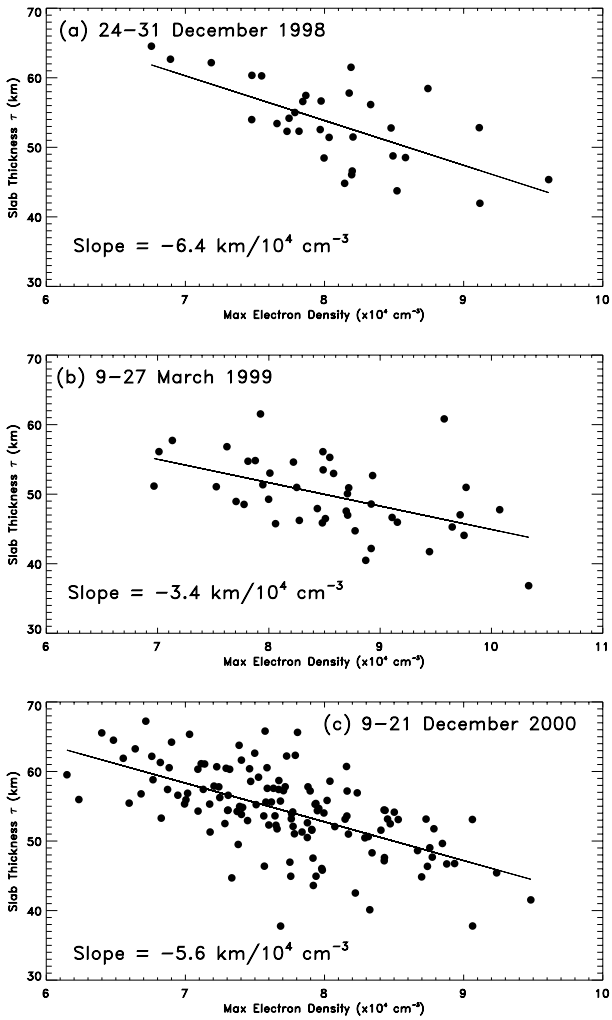

Figure 9. Behavior of equivalent slab thickness (τ) on Mars versus the peak electron density (N_{max}) for the three data sets in Figure 2.

(τ increases from 36 km to 50 km), contrary to the pattern shown in Figure 9. Other causes, such as the neutral atmosphere dynamical effects explored by *Bougher et al.* [2001] and *Forbes* [2002] need to be examined to understand the $N_e(h)$ integral-preserving distortion effects portrayed in Figure 9.

5. Summary and Conclusions

[23] We have examined the first three sets of electron density versus altitude profiles obtained from the MGS radio occultation experiment with the goal of describing their integrated values, or total electron content (TEC), as a way to assess the impact of Mars' ionosphere on potential satellite-based position and navigation systems. The MGS data sets all refer to early local times at high latitudes, arising from solar illumination at high zenith angles, and thus modeling studies were conducted to relate these local measurements to more global morphologies. Photochemical model estimates for the maximum TEC possible on the planet, namely at the subsolar point at perihelion under solar maximum conditions, indicated at most ~2 vertical TEC units (10^{16} el m^{-2}). If sampled along slanted ray paths from orbit to ground, or by satellite-to-satellite ray paths horizontally through the ionosphere, the TEC encountered might be a factor of 2–3 larger. For such upper limit estimates, and for a navigation system using the current GHz/L-band frequencies employed for the terrestrial GPS system, range errors would be of order 1 m. This may be a concern to mission planners, but other uncertainties in precise positioning on Mars might be larger. If the radio beacon frequencies selected for a Mars Communications and Navigation satellite network were much lower (i.e., in the low end of the UHF band), then ionospheric corrections would be of greater relevance. If a dual frequency MC&N system were put into operation at Mars, issues of ionospheric TEC corrections are avoided. Yet, for either solution, it is important to realize that the transmissions themselves would provide a new and extremely valuable diagnostic of the martian ionosphere on a global and continuous basis, providing critical input to ionospheric models and upper atmospheric science, as the current GPS system does on Earth.

[24] Finally, we examined the parameter equivalent slab thickness (τ) for the ionosphere on Mars and found it to vary somewhat more than TEC (opposite to the terrestrial case), and thus not a potentially useful param-

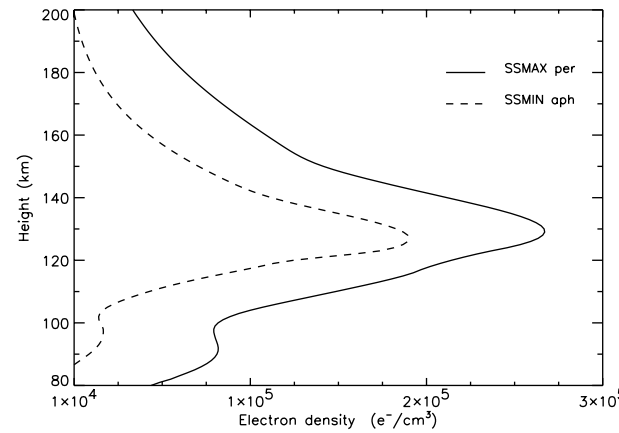

Figure 10. Model results showing $N_e(h)$ profile shape changes at the subsolar point for the extreme cases of Mars at aphelion at solar minimum versus perihelion at solar maximum.

eter to help in global specifications of TEC at Mars. Its anticorrelation with peak electron density, however, points to coupling effects with neutral atmosphere processes not yet understood, and thus further studies, both observationally and via modeling, of slab thickness can advance our scientific understanding of Mars' upper atmosphere.

[25] **Acknowledgments.** The efforts at Boston University were supported, in part, by a grant from the NASA Mars Data Analysis Program, and by seed research funds from the Center for Space Physics. At Stanford University, support for this work came from the Mars Global Surveyor Program. The research conducted at the Jet Propulsion Laboratory, California Institute of Technology, is under a contract with the National Aeronautics and Space Administration.

References

Armand, N. A., V. M. Smirnov, and T. Hagfors (2003), Distortion of radar pulses by the Martian ionosphere, *Radio Sci.*, *38*(5), 1090, doi:10.1029/2002RS002849.

Bougher, S. W., S. Engel, D. P. Hinson, and J. M. Forbes (2001), Mars Global Surveyor radio science electron density profiles: Neutral atmosphere implications, *Geophys. Res. Lett.*, *28*, 3091–3094.

Cesarone, R. J., R. C. Hastrup, D. J. Bell, D. T. Lyons, and K. G. Nelson (1999), Architectural design for a Mars Communications & Navigation orbital infrastructure, paper presented at Astrodynamics Specialist Conference, Am. Astron. Soc., Girwood, Alaska, 16–19 Aug.

Ely, T. A., R. Anderson, Y. E. Bar-Sever, D. Bell, J. Guinn, M. Jah, P. Kallemeyn, E. Levene, L. Romans, and S. Wu (1999), Mars network constellation design drivers and strategies, paper presented at Astrodynamics Specialist Conference, Am. Astron. Soc., Girwood, Alaska, 16–19 Aug.

Fjeldbo, G., W. C. Fjeldbo, and V. R. Eshleman (1966), Models for the atmosphere of Mars based on the Mariner 4 occultation experiment, *J. Geophys. Res.*, *71*, 2307–2316.

Forbes, J. M. (2002), Wave coupling in terrestrial planetary atmospheres, in *Atmospheres in the Solar System: Comparative Aeronomy*, *Geophys. Monogr. Ser.*, vol. 130, edited by M. Mendillo, A. Nagy, and J. H. Waite, AGU, Washington, D. C.

Fox, J. L., P. Zhou, and S. W. Bougher (1995), The Martian thermosphere/ionosphere at high and low solar activities, *Adv. Space Res.*, *17*(11), 203–218.

Fox, M. W., M. Mendillo, and J. A. Klobuchar (1991), Ionospheric equivalent slab thickness and its modeling applications, *Radio Sci.*, *26*, 429–438.

Hantsch, M. H., and S. J. Bauer (1990), Solar control of the Mars ionosphere, *Planet. Space Sci.*, *38*, 539–542.

Hargreaves, J. K. (1992), *The Solar-Terrestrial Environment*, Cambridge Univ. Press, New York.

Hastrup, R. C., R. J. Cesarone, J. M. Srinivasan, and D. D. Morabito (1999), Mars Comm/Nav MicroSat Network, paper presented at 13th Conference on Small Satellites, Am. Inst. of Aeronaut. and Astronaut., Logan, Utah, 23–26 Aug.

Hinson, D. P., R. A. Simpson, J. D. Twicken, and G. L. Tyler (1999), Initial results from radio occultation measurement with Mars Global Surveyor, *J. Geophys. Res.*, *104*, 26,997–27,012.

Hinson, D. P., G. L. Tyler, J. L. Hollingsworth, and R. J. Wilson (2001), Radio occultation measurements of forced atmospheric waves on Mars, *J. Geophys. Res.*, *106*(E1), 1463–1480.

Kliore, A. J. (1992), Radio occultation observations of the ionospheres of Mars and Venus, in *Venus and Mars: Atmospheres, Ionospheres, and Solar Wind Interactions*, *Geophys. Monogr. Ser.*, vol. 66, edited by J. G. Luhmann et al., pp. 265–276, AGU, Washington, D. C.

Krasnopolsky, V. A. (2002), Mars' upper atmosphere and ionosphere at low, medium, and high solar activities: Implications for evolution of water, *J. Geophys. Res.*, *107*(E12), 5128, doi:10.1029/2001JE001809.

Ma, Y., A. F. Nagy, K. C. Hansen, D. L. DeZeeuw, and T. I. Gombosi (2002), Three-dimensional multispecies MHD studies of the solar wind interaction with Mars in the presence of crustal fields, *J. Geophys. Res.*, *107*(A10), 1282, doi:10.1029/2002JA009293.

Martinis, C., J. Wilson, and M. Mendillo (2003), Modeling day-to-day ionospheric variability on Mars, *J. Geophys. Res.*, *108*(A10), 1383, doi:10.1029/2003JA009973.

Melnik, O., and M. Parrot (1999), Propagation of electromagnetic waves through the Martian ionosphere, *J. Geophys. Res.*, *104*, 12,705.

Mendillo, M., J. A. Klobuchar, and H. Hajeb-Hosseinieh (1974), Ionospheric disturbances: Evidence for the contraction of the plasmasphere during severe geomagnetic storms, *Planet. Space Sci.*, *22*, 223–236.

Mendillo, M., S. M. Smith, H. Rishbeth, and D. P. Hinson (2003), Simultaneous ionospheric variability on Earth and Mars, *J. Geophys. Res.*, *108*(A12), 1432, doi:10.1029/2003JA009961.

Nagy, A., and T. Cravens (2002), Solar system ionospheres, in *Atmospheres in the Solar System: Comparative Aeronomy*, *Geophys. Monogr. Ser.*, vol. 130, edited by M. Mendillo, A. Nagy, and J. H. Waite, AGU, Washington, D. C.

Pi, X., C. Wang, G. A. Hajj, G. Rosen, B. D. Wilson, and G. J. Bailey (2003), Estimation of $\mathbf{E} \times \mathbf{B}$ drift using a global assimilative ionospheric model: An observation system simulation experiment, *J. Geophys. Res.*, *108*(A2), 1075, doi:10.1029/2001JA009235.

Rishbeth, H., and O. K. Garriott (1969), *Introduction to Ionospheric Physics*, Academic, San Diego, Calif.

Rishbeth, H., and M. Mendillo (2001), Patterns of *F2* layer variability, *J. Atmos. Sol. Terr. Phys.*, *63*, 1661–1680.

Safaeinili, A., W. Kofman, J.-F. Nouvel, A. Herique, and R. L. Jordan (2003), Impact of Mars ionosphere on orbital radar sounder operation and data processing, *Planet. Space Sci.*, *51*, 505–515.

Schunk, R. W., and A. F. Nagy (2000), *Ionospheres: Physics, Plasma Physics and Chemistry*, Cambridge Univ. Press, New York.

Titheridge, J. E. (1973), The slab thickness of the midlatitude ionosphere, *Planet. Space Sci.*, *21*, 1775–1793.

Titheridge, J. E. (2000), Modeling the peak of the ionospheric *E* layer, *J. Atmos. Sol. Terr. Phys.*, *62*, 93–114.

Tobiska, W. K. (2004), SOLAR 2000 irradiances for climate change, aeronomy, and space system engineering, *Adv. Space Res.*, in press.

Tobiska, W. K., T. Woods, F. Eparvier, R. Viereck, L. Floyd, D. Bouwer, G. Rottman, and O. R. White (2000), The SOLAR 2000 empirical solar irradiance model and forecast tool, *J. Atmos. Sol. Terr. Phys.*, *62*, 1233–1250.

Vignes, D., C. Mazelle, H. Rme, M. H. Acuña, J. E. P. Connerney, R. P. Lin, D. L. Mitchell, P. Cloutier, D. H. Crider, and N. F. Ness (2000), The solar wind interaction with Mars: Locations and shapes of the bow shock and the magnetic pile-up boundary from the observations of the MAG/ER experiment on board Mars Global Surveyor, *Geophys. Res. Lett.*, *27*(1), 49–52.

Witasse, O., J.-F. Nouvel, J.-P. Lebreton, and W. Kofman (2001), HF radio wave attenuation due to a meteoritic layer in the atmosphere of Mars, *Geophys. Res. Lett.*, *28*, 3039–3042.

D. Hinson, Department of Electrical Engineering, Stanford University, Stanford, CA 94305, USA.

C. Martinis, M. Mendillo, S. Smith, and J. Wilson, Center for Space Physics, Boston University, Boston, MA 02215, USA. (mendillo@bu.edu)

X. Pi, Jet Propulsion Laboratory, California Institute of Technology, M/S 138-308, 4800 Oak Grove Drive, Pasadena, CA 91109, USA.